Redox-controlled Backbone Dynamics of Human Cytochrome *c* Revealed by ^{15}N NMR Relaxation Measurements

Koichi Sakamoto[1], Masakatsu Kamiya[2,3], Takeshi Uchida[1,4], Keiichi Kawano[2,3], Koichiro Ishimori[1,4]

[1]*Division of Chemistry, Graduate School of Science, Hokkaido University*
[2]*Graduate School of Life Science, Hokkaido University*
[3]*Faculty of Advanced Life Science, Hokkaido University*
[4]*Department of Chemistry, Faculty of Science, Hokkaido University*

*Corresponding author: Koichiro Ishimori,
Kita 10, Nishi 8, Kita-ku, Sapporo 060-0810, JAPAN
TEL: 81-11-706-2707, FAX: 81-11-706-3501
E-mail: koichiro@sci.hokudai.ac.jp

ABSTRACT

Redox-controlled backbone dynamics in cytochrome *c* (Cyt *c*) were revealed by 2D ^{15}N NMR relaxation experiments. ^{15}N T_1 and T_2 values and ^{1}H-^{15}N NOEs of uniformly ^{15}N-labeled reduced and oxidized Cyt *c* were measured, and the generalized order parameters (S^2), the effective correlation time for internal motion (τ_e), the ^{15}N exchalnge broadening contributions (R_{ex}) for each residue, and the overal correlation time (τ_m) were estimated by model-free dynamics formalism. These dynamic parameters clearly showed that the backbone dynamics of Cyt *c* are highly restricted due to the covalently bound heme that functions as the stable hydrophobic core. Upon the oxidation of the heme iron in Cyt *c*, the average S^2 value was increased from 0.88±0.01 to 0.92±0.01, demonstrating that the mobility of the backbone is further restricted in the oxidized form. Such increases in the S^2 values were more prominent in the loop regions, including amino acid residues near the thioether bonds to the heme moiety and positively charged region around Lys87. Both of the regions are supposed to form the interaction site for cytochrome *c* oxidase (C*c*O) and the electron pathway from Cyt *c* to C*c*O. The redox-dependent mobility of the backbone in the interaction site for the electron transfer to C*c*O suggests an electron transfer mechanism regulated by the backbone dynamics in the Cyt *c* – C*c*O system.

Keywords: cytochrome *c*, backbone dynamics, ^{15}N relaxation, order parameter, electron transfer

Introduction

Cytochrome *c* is a small globular protein that plays an important role in the transfer of electrons in the respiratory chain of mitochondria [1]. It has a *c*-type heme, covalently attached by the two cysteine residues of the peptide via thioether bonds, and mediates electron transfer from Complex III (cytochrome bc_1 complex) to Complex IV (cytochrome *c* oxidase; C*c*O), cycling between the reduced (Fe^{2+}) and the oxidized (Fe^{3+}) forms. Cytochrome *c* can ferry only one electron, while reduction of dioxygen to water molecules catalyzed in C*c*O requires four electrons. After the electron transfer from Cyt *c* to C*c*O, oxidized Cyt *c* is, therefore, supposed to be rapidly dissociated from C*c*O to facilitate the binding of another reduced Cyt *c* for further electron transfer. Although the effective electron transfer from Cyt *c* to C*c*O suggests that the conformational changes are associated with the electron transfer in the Cyt *c*-C*c*O complex [2; 3; 4], the detailed structural and functional analysis of the electron transfer complex between Cyt *c* and C*c*O has not yet been completed due to the large molecular weight of the membrane bound protein complex.

Despite there being no direct structural analysis of the Cyt *c*-C*c*O complex, structural comparisons between the reduced [5] and oxidized Cyt *c* [6] indicate that some structural changes are induced by the oxidation of the heme iron. This finding allows us to speculate that the electron transfer from Cyt *c* to C*c*O would be associated with some conformational changes in Cyt *c*, leading to the "conformationally gated" electron transfer mechanism [4]. The conformational gating during this electron transfer has been the center of focus for many researchers [7; 8; 9], but its molecular mechanism is not fully understood and remains disputed.

One of the keys to elucidating the molecular mechanism of interprotein electron transfer is understanding the dynamic property of the partner proteins. The electron transfer in proteins is significantly affected by their dynamic properties, particularly by the local mobility of the backbone, and the local mobility of the backbone have often been proposed to be important in controlling the electron transfer process [10]. It is suggested to influence both the molecular recognition process and reorganization energy λ, both features being necessary to achieve electron transfer in biological systems. While detailed three-dimensional structures of both of the reduced and oxidized forms of Cyt *c* have been reported [5; 6], information on the local mobility of the backbone of Cyt *c* was limited for the bacterial proteins, where the truncated protein lacking the anchor domain to the membrane was utilized [11]. The significant structural differences between the bacterial and mammalian proteins were reported [12], and thus, the dynamic property of mammalian Cyt *c* is still unclear.

To get insights into the backbone dynamics of the mammalian Cyt *c*, we utilized ^{15}N relaxation from the NMR measurements. The use of ^{15}N relaxation measurements has emerged

as a powerful method to investigate the backbone dynamics of biomolecules across a wide range of timescales at atomic resolution. Based on the three relaxation parameters, longitudinal relaxation time (T_1), transverse relaxation time (T_2) and NOE ratio for each ^{15}N nucleus, we estimated the overall tumbling time, τ_m, the order parameter, S^2, the chemical exchange rate, R_{ex}, and the effective correlation time τ_e, to examine the dynamic properties of the reduced and the oxidized forms of Cyt *c*. Comparison of these dynamic parameters clearly demonstrated the significant differences in the backbone dynamics between the reduced and the oxidized forms of Cyt *c*, suggesting the redox-controlled dynamic property of Cyt *c*.

Material and Methods

The expression and purification of ^{15}N-labeled human Cyt *c* was followed by the previous study with some modifications [13]. The purified protein with an R-value (=A_{409}/A_{280}) of over 4.5 was dissolved into 50 mM sodium phosphate buffer at pH 7.0 by centrifugal ultrafiltration.

NMR samples for the ^{15}N relaxation measurements were prepared containing 0.4 mM ferrous ^{15}N-labeled Cyt *c* in 50 mM sodium phosphate buffer with 0.2% DM and 5% D_2O, and the pH was adjusted to 6.8. All ^{15}N NMR experiments were performed at 293 K on a Bruker Avance 600 equipped with a cryogenic triple resonance probe. The spectral processing was done following the procedures in previous studies [14; 15]. The relaxation data sets were fit to the axially symmetric model-free spectral density function using a model-free program [16; 17].

Results and Discussion

Relaxation parameters of the reduced and the oxidized forms of Cyt c

To determine the T_1 and T_2 for each ^{15}N nucleus, we measured the T_1 and T_2 spectra of the reduced and oxidized forms of Cyt *c*. In the reduced form of Cyt *c*, the peaks from Gly1, His18, Glu21, Thr28, Pro30, Asn31, Pro44, Gly45, Gly56, Pro71, Pro76, and Leu84 were excluded from further analysis due to low intensity or an unresolved peak. Out of the 99 residues, excluding 4 Pro residues and the N-terminal residue, 92 amino acid residues were used for the relaxation analysis of the reduced form of Cyt *c*. In the oxidized form of Cyt *c*, the excluded peaks were Gly1, Glu21, His26, Thr28, Pro30, Pro44, Gly45, Gly56, Pro71, Pro76, Leu84, and Asp93. The 92 residues were also used for the determination of the relaxation parameters in the oxidized form. The T_1 and T_2 values were obtained from fitting the data to an exponential decay using the Sparky program (T. D. Goddard and D. G. Kneller, SPARKY 3, University of California, San Francisco), and the typical T_1 and T_2 relaxation decay curves are shown in Figure 1. The calculated T_1 and T_2 values in the reduced and oxidized forms were then converted into the R_1 and R_2 rate constants and plotted in Figures 2 (a), (b), (d) and (e). The average values of R_1 and R_2 in reduced Cyt *c* were 1.43 ± 0.02 and 11.2 ± 0.52 s^{-1}, and in oxidized Cyt *c*, the average R_1 value was increased to 1.84 ± 0.02 s^{-1}, while the averaged R_2 value was decreased to 9.42 ± 0.52 s^{-1}.

In addition to the R_1 and R_2 rates, the steady state ^1H-^{15}N NOE spectra were also measured in both reduced and oxidized Cyt *c*. The intensities of the NOE peaks were estimated with the Sparky program, and the NOE ratios of the two states were calculated using the peak intensities in the presence and absence of proton saturation. Figures 2 (c) and (f) show the NOE ratios of reduced and oxidized Cyt *c*, and the averaged NOE values of reduced and oxidized Cyt *c* were 0.84 ± 0.02 and 0.86 ± 0.01, respectively.

Dynamic parameters from model-free analysis

Based on the entire set of experimental relaxation data, dynamic parameters (τ_m, S^2, τ_e, and R_{ex}) have been obtained for reduced and oxidized Cyt *c*. Optimal τ_m, the overall tumbling time, of reduced and oxidized Cyt *c* were determined to be 6.08 ± 0.02 and 6.16 ± 0.01 ns, respectively, which are in good agreement with correlation times for other proteins of the similar size [18]. The τ_m value of reduced Cyt *c* is not so different from that of oxidized Cyt *c*, indicating that the overall rotational motion in reduced Cyt *c* is nearly the same as that in the

oxidized form. The similarity in the correlation times of the two forms also suggests that the paramagnetic effect in the oxidized form is negligible for the parameters of the relaxation, and the paramagnetic effects on the relaxation parameters can, therefore, be neglected in calculating the model-free parameters.

By using these τ_m values, the order parameter, S^2, which reflects the amplitude of internal motion on a nanosecond-picosecond timescale, the chemical exchange rate, R_{ex}, which indicates the presence of conformational exchange on a slow timescale, and τ_e, which represents the values of the effective correlation time, were calculated and plotted as a function of the amino acid sequence in Figure 3. The average S^2 values for the helices and loop structures in reduced and oxidized Cyt *c* are listed in Table 1.

Backbone dynamics of reduced and oxidized Cyt c

As clearly shown in Table 1, the average values of S^2 for reduced and oxidized Cyt *c* were 0.88 ± 0.01 and 0.92 ± 0.01, respectively. As predicted from the compressibility [19], Cyt *c* exhibits higher S^2 values, corresponding to more rigid structures than other proteins. In the reduced state, only eight amino acid residues showing $S^2 \leq 0.80$ (Val3, Thr19, Val20, His26, Lys27, Gln42, Ile57, and Asn70) were observed, which are located in the loop regions. However, the average S^2 value of the loop regions (S^2_{red}(L) = 0.855) is still higher than those in the SH3 domain (S^2 = 0.76) [18] and calbindin (S^2 = 0.59) [15], comparable those in their helices. Such restricted mobility of the backbone would be derived from the characteristic structure of Cyt *c*. One of the characteristics of the Cyt *c* structure is the covalently attached heme group. Heme is highly hydrophobic, serving as the stable hydrophobic core in the metalloproteins, and both of the hydrophilic propionate groups are thioesterified to Cys residues of the peptide to fix the hydrophobic core in the protein matrix of Cyt *c*. In addition, the loop regions have hydrogen-bonding networks [5; 6], also restricting the mobility of the backbone.

The restricted backbone dynamics of Cyt *c* were also suggested by the chemical exchange rates, R_{ex}, as illustrated in Figure 2 (b). The structural multiplicity in the micro- to millisecond region was detected in the loop regions, but only in the L3 and L4 loop regions. The L3 loop is the more flexible loop, consisting of more than 30 amino acid residues (Table 1). The lower steric constraint of the backbone would result in structural multiplicity. The L6 and L7 loop regions, which are also relatively long loop regions, showed less structural multiplicity. Chemical exchange was observed for only two residues (Lys79 and Ile81) in these loop regions, and the S^2 values of the L6 (S^2_{red} = 0.887) and L7 (S^2_{red} = 0.874) loop regions are also higher than those of the other loop regions. Although the structural factors that restrict the backbone

dynamics in these loop regions are still unclear, Met80, which is located in the middle of the L6 and L7 loops, is one of the axial ligands for the heme. The ligation of the heme would reduce the flexibility of the backbone in these loop regions.

Another parameter deduced from the relaxation experiments is τ_e. As shown in Figure 2 (c), only two amino acid residues (Lys39 and Lys87) exhibited detectable effective internal motion, which is in sharp contrast to the results of putidaredoxin, an example of an iron-sulfur electron transfer [20]. In putidaredoxin, the effective internal motion was detected for 44 and 41 of 106 amide nitrogens in the reduced and oxidized forms, respectively. Very few amino acid residues showing detectable effective internal motion also correspond to the restricted backbone dynamics of Cyt *c*.

In the oxidized form, the average S^2 value of the loop regions is enhanced to 0.915, which is even higher than those of typical helices, and the mobility of the loop regions in oxidized Cyt *c* is more depressed than that of the reduced form. Such enhancement of restriction of the backbone dynamics upon the oxidation of the heme iron are also found in the helix regions. The helix regions in the reduced form of Cyt *c* showed $S^2_{red}(H) = 0.914$, while the average values for those in the oxidized form were still higher, with $S^2_{ox}(H) = 0.929$. Thus, the entire backbone dynamics of oxidized Cyt *c* are highly restricted.

Optimization of the amide nitrogens of the oxidized form required R_{ex} terms for 23 residues (Figure 2 (e)), which is increased from that of the reduced form (18 residues). The chemical exchanges correspond to the conformational fluctuation of the backbone at a longer time scale or the flip-flop motions of the aromatic ring of the side chain. In some of the non-aromatic amino acid residues showing the chemical exchange (Gly23 and Lys39), the exchange rates are significantly retarded upon the oxidation, while the chemical exchanges in the L7 loop region (Val83, Lys86, and Lys88) were detected only in oxidized Cyt *c*. The dynamic property of Cyt *c* at a longer time scale also depends on the redox state of the heme iron. The effective internal motion was also detected for only two terminal residues (Glu4 and Glu104) (Figure 2 (f)), but these amino acid residues are different from those in the reduced form. The structural multiplicity in the oxidized form is also significantly different from that in the reduced form.

Comparison of backbone dynamics between reduced and oxidized Cyt c

To delineate the difference in the backbone dynamics between reduced and oxidized Cyt *c*, the changes of the S^2 values upon the oxidation ($\Delta S^2 = S^2_{ox} - S^2_{red}$) were plotted against the amino acid sequence, as illustrated in Figure 4. As is clearly shown in Figure 4, most of the amino acid

residues showed positive ΔS^2 values, corresponding to more restricted flexibility in the oxidized form. Enhancement of the values was prominent in the amino acid residues of the loop regions. In these amino acid residues in which the backbone flexibility was decreased upon oxidation of the heme, we noted that Cys14, one of the Cys residues that is thioether-bridged to the heme, showed a large increase in the S^2 value ($\Delta S^2 > 0.1$). Gln16, which is located between the two thioether bonds of Cys14 and Cys17, also showed a highly enhanced S^2 value upon the oxidation. The backbone dynamics around the thioether bonds are significantly restricted by the oxidation of the heme iron.

It is quite interesting that the mutation of Lys13, which is the amino acid residue adjacent to Cys 14, resulted in the severe suppression of electron transfer from Cyt *c* to C*c*O [21] and plays a key role in the electron transfer [22; 23]. Molecular simulation for the formation of the Cyt *c* – C*c*O complex also revealed that the exposed heme moiety site around the thioether bonds can form the interaction site for C*c*O [24]. Although the backbone dynamics of Lys13 are almost insensitive to the oxidation, we can suggest that the decrease in the flexibility of the backbone around the thioether bonds is closely related to the electron transfer from Cyt *c* to C*c*O, which allows us to speculate on the regulation mechanism of electron transfer by the backbone dynamics of Cyt *c*.

Such a correlation of dynamic property changes and electron transfer is also supported by the enhancement of the S^2 value of the L6 and L7 loop regions. This region has a positively charged region that contains several Lys residues [5; 6] that are considered to be the potential interaction site for the negatively charged region of subunit II in C*c*O [24]. The backbone fluctuations of these loop regions on the picosecond - nanosecond timescales were suppressed for the oxidized form relative to the reduced form. While the timescale of the backbone dynamics we estimated here are quite fast, previous study also revealed that the amino acid residues in the interaction site for the partner protein show the redox-dependent picosecond - nanosecond backbone dynamics and suggested the electron transfer regulated by the redox-dependent backbone dynamics [20]. Although we cannot exclude the possibility that the binding of C*c*O might significantly perturb the dynamic properties of Cyt *c*, the site-specific changes of the backbone dynamics in the interaction site for C*c*O upon the oxidation strongly suggest that the redox-dependent dynamic property would have some advantages for dissociation of the Cyt *c*-C*c*O complex to facilitate the successive electron transfer to C*c*O.

In addition to the fast motions, the changes in the internal slow motions on the microsecond - millisecond timescale were also induced in the L7 loop region, concomitant with oxidation of the heme iron. As shown in Figures 3 (b) and (e), slow fluctuations of the backbone of Lys86 and Lys88, both of which are involved in the positively charged region, were

detected only in oxidized Cyt *c*. The contribution of these residues to the electron transfer to C*c*O is also evident by our preliminary kinetic results of the electron transfer. The K_M value of the K86/87L Cyt *c* mutant for the electron transfer complex between Cyt *c* and C*c*O were larger than that of wild-type Cyt *c*. Internal slow motions disappeared for Lys79 and Ile81 in the oxidized form. Although further experiments are required to draw a definitive relationship between the slow motion and the Cyt *c* - C*c*O complex formation, it is likely that slow motions in the positively charged region play important roles in the interaction between C*c*O and Cyt *c*.

While these redox-dependent backbone dynamics would be a key to understanding the molecular mechanism of interprotein electron transfer, we have not yet found out how the redox state modulates the dynamics of Cyt *c*. Some of the electron transfer proteins showed different backbone dynamics between the reduced and oxidized forms, but they cannot be generalized as the difference in backbone mobility between the oxidized and reduced forms has been found to be either positive of negative [25; 26]. Upon the oxidation of the heme iron in reduced Cyt *c*, the Fe – Met80 bond, one of the axial bonds of the heme-iron, is strengthened due to the higher affinity of the sulfur atom to the ferric iron than the ferrous iron [27], and the S (Met80) – Fe (heme) – N (heme) bond angle becomes more close to the perpendicular orientation [5; 6]. The strengthened Fe – Met80 bond would reduce the backbone mobility of the L6 and L7 loop region in oxidized Cyt *c*.

In conclusion, by analyzing the ^{15}N relaxation of the backbone of Cyt *c* based on the model-free program, we successfully obtained the microscopic views of the redox-dependent backbone changes over picosecond to millisecond timescales. Upon oxidation of reduced Cyt *c*, we found that the backbone fluctuations on the picosecond - nanosecond timescales were significantly suppressed in the exposed heme moiety around the thioether bonds and the positively charged region, both of which are the supposed interaction sites for C*c*O. We also found that the slow motions on the microsecond - millisecond timescales were changed in the L7 loop region. The dynamic parameters of reduced and oxidized Cyt *c* that we present here clearly indicate the redox-controlled backbone dynamics in the interaction site for the electron transfer to C*c*O, suggesting that the electron transfer is regulated by the dynamic conformational properties of Cyt *c*.

Acknowledgements

We thank Professor A Grant Mauk (University of British Columbia) for his helpful suggestions on the expression of Cyt *c*. This work was supported by Grants-in-Aid for Scientific Research (21370040) and Scientific Research on Priority Areas (20051002).

References

[1] G.W. Pettigrew, and G.R. Moore, Cytochrome *c* - Biological Aspects, Springer-Verlag, Berlin, 1987.

[2] C. Weber, B. Michel, and H.R. Bosshard, Spectroscopic analysis of the cytochrome *c* oxidase-cytochrome *c* complex: circular dichroism and magnetic circular dichroism measurements reveal change of cytochrome *c* heme geometry imposed by complex formation. Proc. Natl. Acad. Sci. USA 84 (1987) 6687-6691.

[3] S.L. Mayo, W.R. Ellis Jr, R.J. Crutchley, and H.B. Gray, Long-range electron transfer in heme proteins Science 233 (1986) 948-952.

[4] J.R. Winkler, B.G. Malmström, and H.B. Gray, Rapid electron injection into multisite metalloproteins: intramolecular electron transfer in cytochrome oxidase. Biophys. Chem. 54 (1995) 199-209.

[5] L. Banci, I. Bertini, J.G. Huber, G.A. Spyroulias, and P. Turano, Solution structure of reduced horse heart cytochrome *c*. J. Bioinorg. Chem. 4 (1999) 21 - 31.

[6] L. Banci, I. Bertini, H.B. Gray, C. Luchinat, T. Reddig, A. Rosato, and P. Turano, Solution structure of oxidized horse heart cytochrome *c*. Biochemistry 36 (1997) 9867 - 9877.

[7] V.L. Davidson, What Controls the Rates of Interprotein Electron-Transfer Reactions. Accounts of Chemical Research 33 (2000) 87-93.

[8] F.I. Rosell, J.C. Ferrer, and A.G. Mauk, Proton-linked protein conformational switching: Definition of the alkaline conformational transition of yeast *iso*-1-ferricytochrome *c*. J. Am. Chem. Soc. 120 (1998) 11234-11245.

[9] E.S. Medvedev, A.I. Kotelnikov, A.V. Barinov, B.L. Psikha, J.M. Ortega, D.M. Popovic, and A.A. Stuchebrukhov, Protein dynamics control of electron transfer in photosynthetic reaction centers from *Rps. Sulfoviridis*. J. Phys. Chem. B 112 (2008) 3208-3216.

[10] G.W. Canters, and M. van de Kamp, Protein-mediated electron transfer. Current Opinion in Structural Biology 2 (1992) 859-869.

[11] B. Reincke, C. Pérez, P. Pristovšek, C. Lücke, C. Ludwig, F. Löhr, V.V. Rogov, B. Ludwig, and H. Rüterjans, Solution structure and dynamics of the functional domain of *Paracoccus denitrificans* cytochrome c_{552} in both redox states. Biochemistry 40 (2001) 12312-12320.

[12] E.A. Berry, and B.L. Trumpower, Isolation of ubiquinol oxidase from *Paracoccus denitrificans* and resolution into cytochrome bc_1 and cytochrome c-aa_3 complexes. J. Biol. Chem. 260 (1985) 2458-2467.

[13] W.-Y. Jeng, C.-Y. Chen, H.-C. Chang, and W.-J. Chuang, Expression and Characterization of Recombinant Human Cytochrome *c* in *E. coli*. J. Bioenerg. Biomem. 34 (2002) 423-431.

[14] F. Delaglio, S. Grzesiek, G.W. Vuister, G. Zhu, J. Pfeifer, and A. Bax, NMRPipe: a multidimensional spectral processing system based on UNIX pipes. J. Biomol. NMR 6 (1995) 277-293.

[15] J. Kördel, N.J. Skelton, M. Akke, A.G. Palmer III, and W.J. Chazin, Backbone dynamics of calcium-loaded calbindin D_{9k} studied by two-dimensional proton-detected ^{15}N NMR spectroscopy. Biochemistry 31 (1992) 4856-4866.

[16] A.M. Mandel, M. Akke, and A.G. Palmer III, Backbone dynamics of *Escherichia coli* ribonuclease HI: Correlations with structure and function in an active enzyme. J. Mol. Biol. 246 (1995) 144-163.

[17] A.M. Mandel, M. Akke, and A.G. Palmer III, Dynamics of Ribonuclease H: Temperature Dependence of Motions on Multiple Time Scales. Biochemistry 35 (1996) 16009-16023.

[18] N.A. Farrow, O. Zhang, J.D. Forman-Kay, and L.E. Kay, Characterization of the backbone dynamics of folded and denatured states of an SH3 domain. Biochemistry 36 (1997) 2390-2402.

[19] K. Gekko, and Y. Hasegawa, Compressibility-structure relationship of globular proteins. Biochemistry 25 (1986) 6563-6571.

[20] N. Sari, M.J. Holden, M.P. Mayhew, V.L. Vilker, and B. Coxon, Comparison of backbone dynamics of oxidized and reduced putidaredoxin by ^{15}N NMR relaxation measurements. Biochemistry 38 (1999) 9862-9871.

[21] H.T. Smith, N. Staudenmayer, and F. Millett, Use of specific lysine modifications to locate the reaction site of cytochrome *c* with cytochrome oxidase. Biochemistry 16 (1977) 4971-4974.

[22] S. Ferguson-Miller, D.L. Brautigan, and E. Margoliash, Definition of cytochrome *c* binding domains by chemical modification. III. Kinetics of reaction of carboxydinitrophenyl cytochromes *c* with cytochrome *c* oxidase. J. Biol. Chem. 253 (1978) 149-159.

[23] K. Niki, W.R. Hardy, M.G. Hill, H. Li, J.R. Sprinkle, E. Margoliash, K. Fujita, R. Tanimura, N. Nakamura, H. Ohno, J.H. Richards, and H.B. Gray, Coupling to lysine-13 promotes electron tunneling through carboxylate-Terminated alkanethiol self-assembled monolayers to cytochrome *c*. J. Phys. Chem. B 107 (2003) 9947-9949.

[24] I. Bertini, G. Cavallaro, and A. Rosato, A structural model for the adduct between cytochrome *c* and cytochrome *c* oxidase. J. Biol. Inorg. Chem. 10 (2005) 613-624.

[25] M. Assfalg, L. Banci, I. Bertini, S. Ciofi-Baffoni, and P.D. Barker, ^{15}N Backbone Dynamics of Ferricytochrome b_{562}: Comparison with the Reduced Protein and the R98C Variant. Biochemistry 40 (2001) 12761-12771.

[26] B. Dangi, Sarma, S., Yan, C., Banville, D. L., Guiles, R. D., The Origin of Difference in the Physical Properties of the Equilibrium Forms of Cytochrome b_5 Revealed through High-Resolution NMR Structures and Backbone Dynamic Analysis. Biochemistry 37 (1998) 8289 - 8302.

[27] S. Adachi, S. Nagano, K. Ishimori, Y. Watanabe, I. Morishima, T. Egawa, T. Kitagawa, and R. Makino, Roles of proximal ligand in heme proteins: replacement of proximal histidine of human myoglobin with cysteine and tyrosine by site-directed mutagenesis as models for P-450, chloroperoxidase, and catalase. Biochemistry 32 (1993) 241-252.

Figure Legends

Figure 1. Examples of T_1 (a: reduced, c: oxidized) and T_2 (b: reduced, d: oxidized) relaxation decay curves for selected residues in reduced Cyt *c*. Resonance peak intensities are plotted against time, and curves indicate fitting to single-exponential decays. Error bars are smaller than the size of characters used to indicate data points. T_1 and T_2 data derived from Lys7(亘), Cys17(☷), Lys87(`), and Glu90(♆) are shown.

Figure 2. Experimental values for relaxation rates, R_1 (=1/T_1), R_2 (=1/T_2), and NOE ratios are shown for the reduced form (a), (b), (c) and oxidized form (d), (e), (f) of Cyt *c*, plotted as a function of residue number. Gaps in the data result from overlapping resonances, broadened resonances, and unassigned resonances that made measurements unavailable.

Figure 3. Plots of the optimized model-free parameters as a function of residue number for ferrous and ferric Cyt *c*. Panels (a) to (c) are for reduced Cyt *c* and panels (d) to (f) are for oxidized Cyt *c*. Optimized values of the generalized order parameters (S^2) are shown in panels (a) and (d), exchange parameters (R_{ex}) are shown in panels (b) and (e), and values of effective correlation time (τ_e) are shown in panels (c) and (f).

Figure 4. Plots of difference of S^2 between the oxidized and reduced forms ($\Delta S^2 = S^2_{ox} - S^2_{red}$) as a function of residue number for Cyt *c*.

Figure 1.

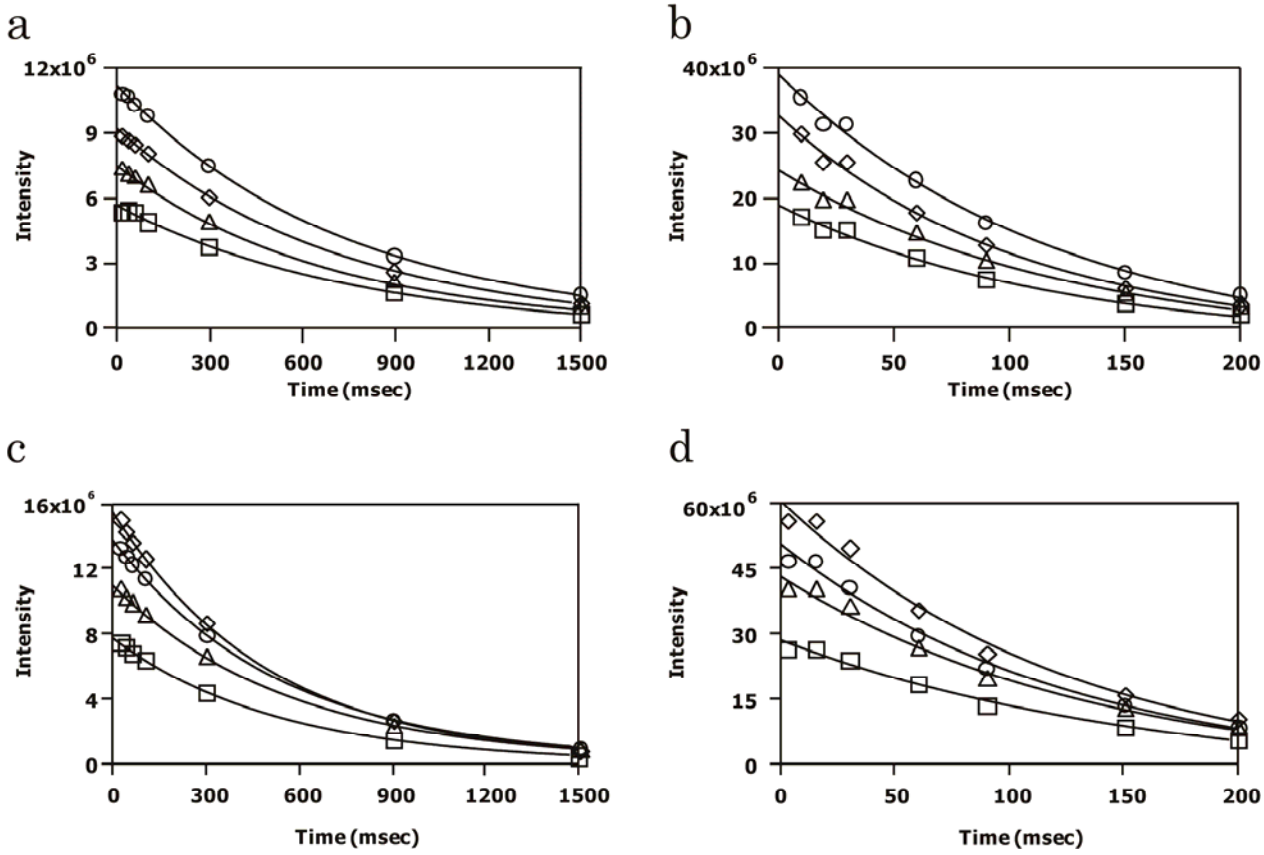
a
12x10^6
9
6
3
0
Intensity
0
300
600
900
1200
1500
Time (msec)
b
40x10^6
30
20
10
0
Intensity
0
50
100
150
200
Time (msec)
c
16x10^6
12
8
4
0
Intensity
0
300
600
900
1200
1500
Time (msec)
d
60x10^6
45
30
15
0
Intensity
0
50
100
150
200
Time (msec)

Figure 2.

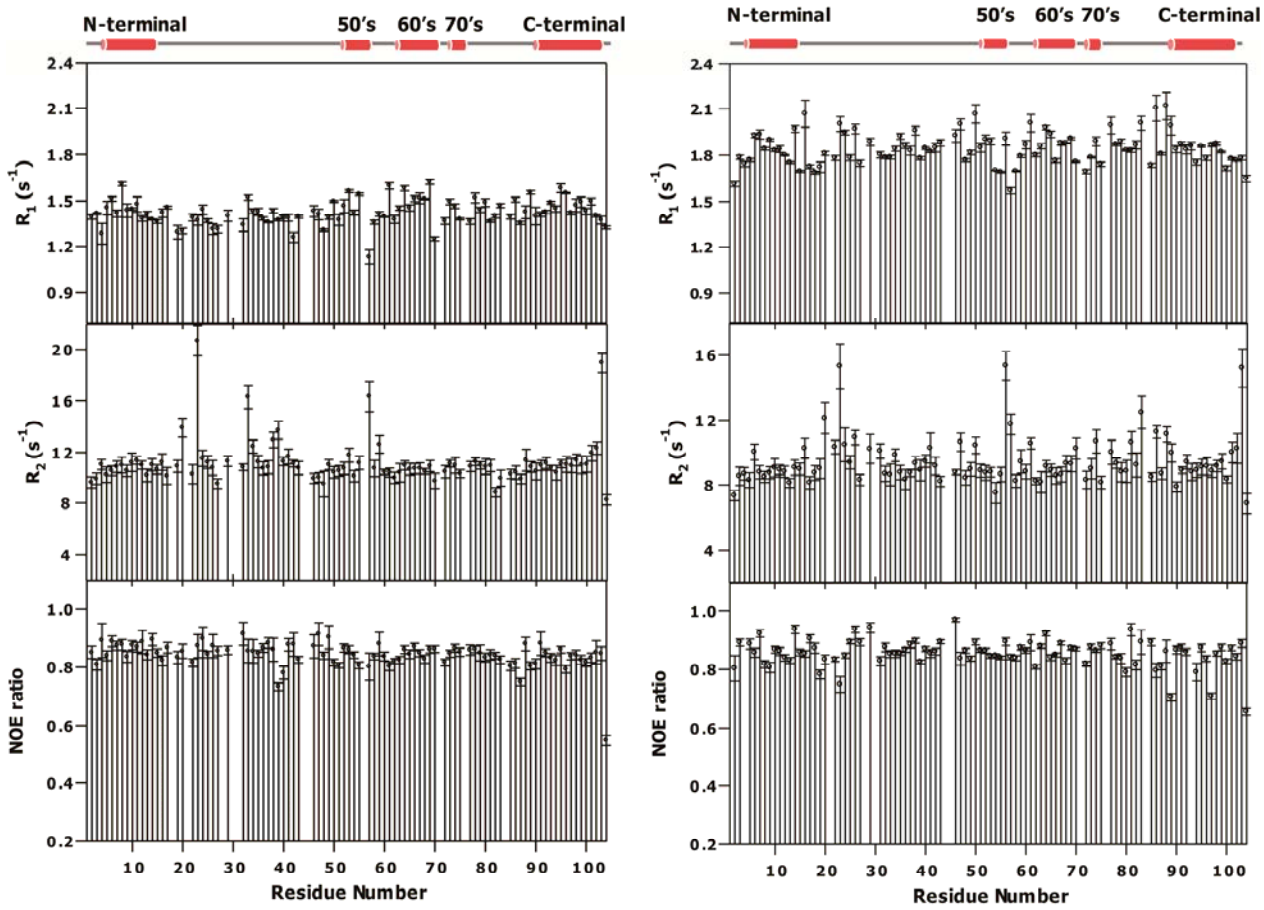
N-terminal
50's
60's
70's
C-terminal
R1 (s-1)
R2 (s-1)
NOE ratio
Residue Number
N-terminal
50's
60's
70's
C-terminal
R1 (s-1)
R2 (s-1)
NOE ratio
Residue Number

Figure 3.

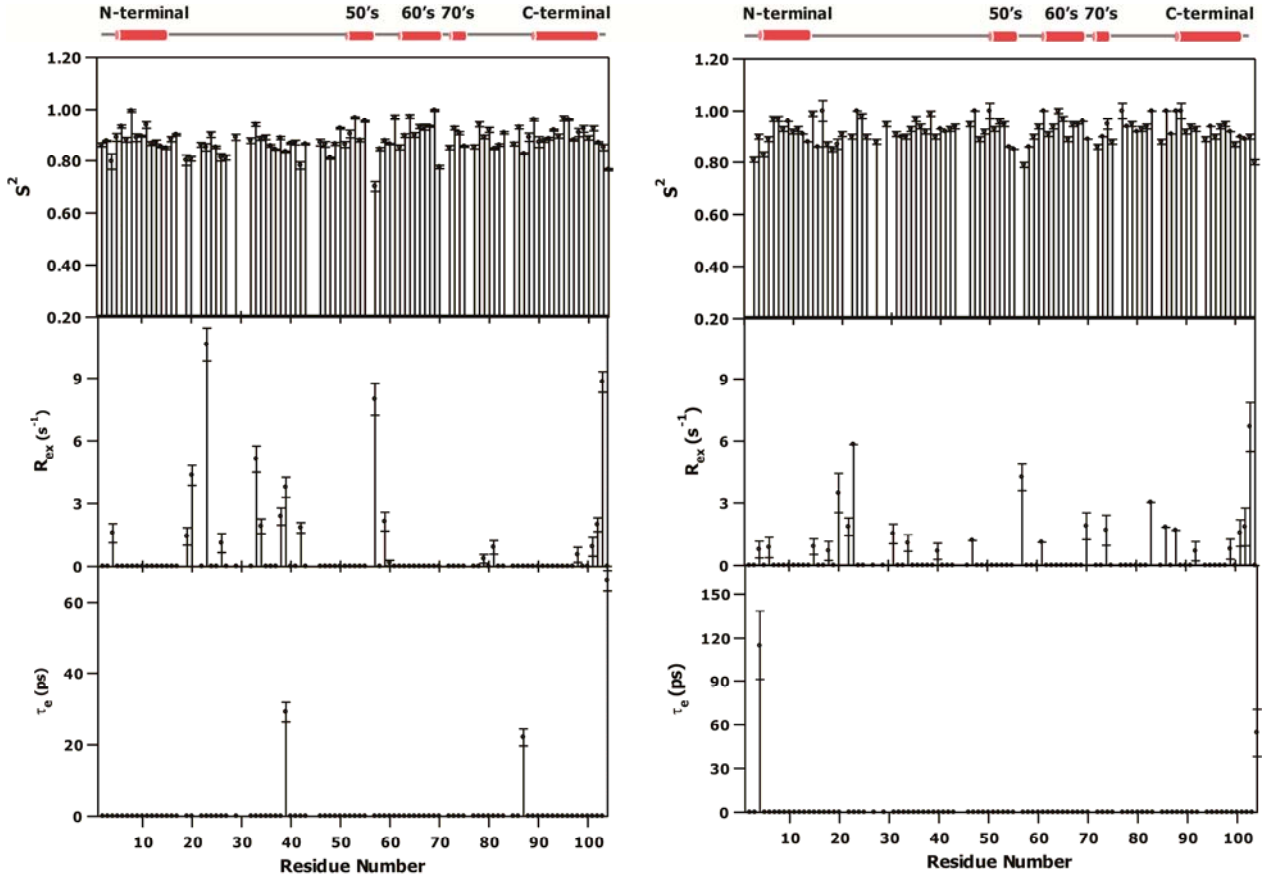
N-terminal
50's
60's 70's
C-terminal
S2
Rex (s-1)
τe (ps)
Residue Number
N-terminal
50's
60's 70's
C-terminal
S2
Rex (s-1)
τe (ps)
Residue Number

Figure 4.

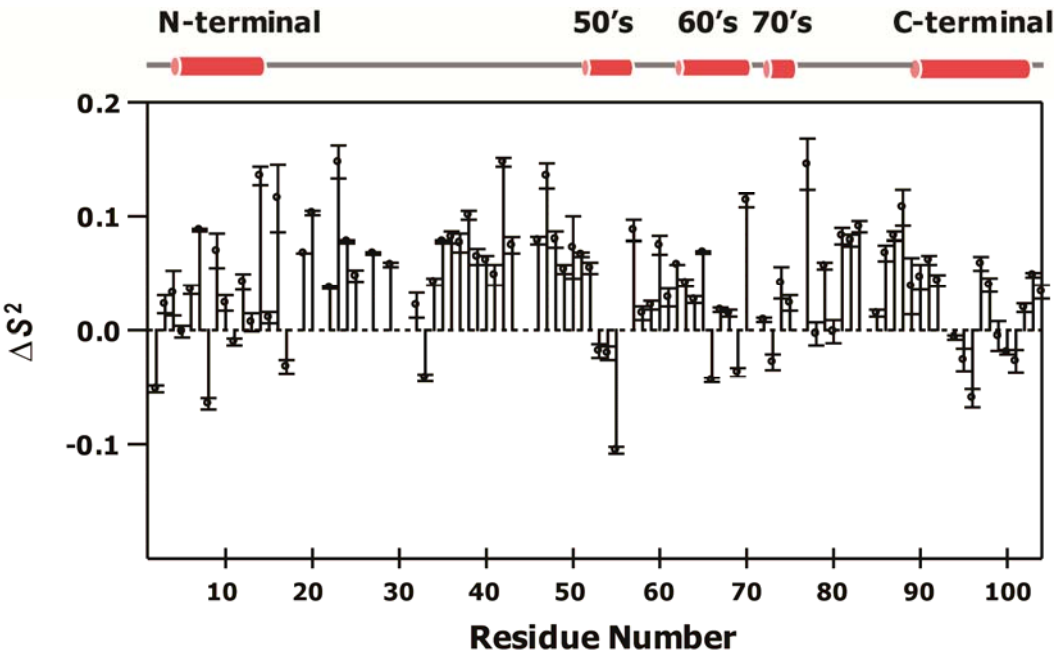
N-terminal
50's
60's
70's
C-terminal
0.2
0.1
0.0
-0.1
ΔS²
10
20
30
40
50
60
70
80
90
100
Residue Number

Table 1. Average order parameter values (S^2) for structural elements of reduced and oxidized Cyt *c*

Residues	Structural Elements	Reduced Cyt *c* (S^2_{red})	Oxidized Cyt *c* (S^2_{ox})	ΔS^2 ($S^2_{ox} - S^2_{red}$)
1 – 2	L1	0.862	0.810	– 0.052
3 – 13	H1	0.905	0.917	+ 0.012
14	Cys (thioether)	0.854	0.990	+ 0.145
15 – 16	L2	0.867	0.860	– 0.007
17	Cys (thioether)	0.902	0.870	– 0.032
18	His (axial ligand)	–	0.850	–
19 – 49	L3	0.857	0.929	+ 0.072
50 – 55	H2	0.916	0.925	+ 0.009
56 – 60	L4	0.823	0.873	+ 0.050
61 – 69	H3	0.933	0.952	+ 0.019
70	L5	0.776	0.890	+ 0.114
71 – 74	H4	0.896	0.903	+ 0.007
75 – 79	L6	0.887	0.942	+ 0.055
80	Met (axial ligand)	0.921	0.920	– 0.001
81 – 87	L7	0.874	0.943	+ 0.069
88 – 101	H5	0.912	0.931	+ 0.017
102 – 104	L8	0.829	0.863	+ 0.034
average		0.883	0.921	+ 0.038